CHARACTERIZATION AND ANALYSIS OF CIGS AND CdTe SOLAR CELLS

Annual Report

Phase II

February 1, 2006 – January 31, 2007

by

James R. Sites
Department of Physics
Colorado State University
Fort Collins, Colorado 80523

Work performed under Subcontract XXL-5-44205-03
National Renewable Energy Laboratory
1617 Cole Boulevard
Golden, Colorado 80401

SUMMARY

A number of studies relating to the fundamental operation of CIGS and CdTe solar cells were performed during Phase II. In addition, we have worked closely with industrial and NREL partners to evaluate specific cells, expanded our quantum efficiency capabilities, and analyzed the average annual efficiency to be expected from several commercial thin-film modules.

The fundamental work on CIGS cells included an analysis of the expected behavior for submicron absorbers. A baseline scenario based on experimental results was compared with conditions where the absorber lifetime and its carrier concentration were reduced by an order of magnitude. Additional calculations compared front-side with back-side illumination, again in the context of experimental results, and calculated several consequences of weak-diode areas and partial shunting, both expected to be of increasing importance for thinner CIGS. Finally, a collaboration with NREL compared the differences between 19.5%-efficient CdZnS/CIGS cells and those made with the conventional CdS buffer.

A major CdTe project in response to the excessive voltage deficit between CdTe and single-crystal cells has been the analysis of strategies to significantly enhance voltage. One strategy recommended for a major experimental effort is an n-i-p structure with an electron reflector before the back contact. Experimentally, CdTe lifetime and current-voltage curves were measured as a function of copper amount used in the back contact, and the expected impact of low lifetimes, including artificially large A-factors, was calculated. Also, experimentally, CdTe cells made with commercially compatible processing were utilized to determine how CdS thickness affects the cell performance parameters.

TABLE OF CONTENTS

SUMMARY 2

FIGURES AND TABLES 4

INTRODUCTION 5

BASIC CIGS STUDIES 6

Thin CIGS Absorbers 6
CIGS Nonuniformities 10
High-Effiency CdZnS/CIGS 13

BASIC CdTe STUDIES 14

Voltage Deficit 15
Absorber Lifetime 19
Thin CdS 22

GENERAL STUDIES 25

QE Under Light Bias 25
Effective Module Efficiency 26
Industrial Impact 28

PHASE III PLANS 29

COMMUNICATIONS 30

Publications 30
Presentations 31
Degrees 32

FIGURES

Figure 1. Impact of absorber thickness on CIGS cell parameters 6
Figure 2. CIGS J-V parameters for three grading profiles 7
Figure 3. CIGS J-V parameters for front and back illumination 9
Figure 4. CIGS QE for front and back illumination 10
Figure 5. Schematic of diode network model 11
Figure 6. Weak-diode voltage maps for low and high series resistance 12
Figure 7. Efficiency dependence on weak-diode parameters 13
Figure 8. Comparison of poly- and single-crystal J-V curves 15
Figure 9. CdTe band diagram: three cases 17
Figure 10. Calculated n-p CdTe voltage vs. carrier density and lifetime 18
Figure 11. Calculated CdTe voltage for n-i-p structure 18
Figure 12. Two approaches to higher CdTe voltage 19
Figure 13. Calculated CdTe J-V as a function of lifetime 20
Figure 14. Artificial enhancement of A-factor at small lifetimes 21
Figure 15. CdTe J-V for different amounts of back-contact copper 22
Figure 16. CdTe TRPL curves as a function of Cu thickness 22
Figure 17. Variation in CdTe QE response with CdS thickness 23
Figure 18. CdTe J-V parameters vs. CdS thickness 24
Figure 19. LBIC comparison of thin and intermediate thickness CdS. 24
Figure 20. Small bias-light effect on measured QE 25
Figure 21: Strong QE dependence on bias light with secondary barrier 26

INTRODUCTION

The work reported here embodies a device-physics approach based on careful measurement and interpretation of data from $CuIn_{1-x}Ga_xSe_2$ (CIGS) and CdTe solar cells. The project goals have been (1) to reliably and quantitatively separate individual performance loss mechanisms, (2) to expand the tools available for such measurement and analysis, (3) to refine the physical explanations for performance losses, and (4) to suggest fabrication approaches or modifications that can reduce these losses. Device physics provides the link between basic materials properties and solar-cell performance. It allows us to be quantitative, it gives a rational framework for choosing research directions, and it often serves as a reality check for proposed solar-cell models.

The experimental and analytical work in this report has largely been done by a dedicated group of graduate students. Samuel Demtsu and Caroline Corwine, who completed their PhD degrees in 2006, explored the impact of copper on both the back contact and the bulk CdTe (Samuel) and the PL signatures related to copper and oxygen in CdTe (Caroline). Ana Kanevce has focused on thin CIGS absorbers, including the increased importance of non-uniformities and the possibilities for rear illumination. Jun Pan has shown how the interplay between absorber lifetime and back-contact barrier leads to the different J-V signatures seen in CdTe cells and how one might significantly increase the voltage of CdTe cells. Tim Nagle has shown how to extract useful information from light-biased QE, and Alan Davies has explored the viability of thin CdS with commercial CdTe processes. In addition, Prof. Alan Fahrenbruch has assisted with several aspects of CdTe device physics, and Prof. Marko Topič has collaborated with us on the effective efficiency of modules under field conditions.

Prof. Sites' group has actively participated in the NREL-sponsored National CIGS and CdTe R&D Teams. It has a very productive collaboration with Prof. Sampath's group at Colorado State, and various levels of collaboration and information exchange with colleagues from AVA, CSM, First Solar, Heliovolt, IEC, ISET, Miasole, Nanosolar, NREL, SoloPower, Solyndra, Ljubljana (Slovenia), USF, and Toledo.

BASIC CIGS STUDIES

Thin CIGS Absorbers. There are several advantages to reducing CIGS absorber thickness. However, one would generally expect the efficiency to decrease at smaller absorber thicknesses. Several groups have shown this to be the case for CIGS cells [Negami et al, Proc. 2nd WCPEC (1998) p. 1181; Lundberg et al, Prog. Photovoltaics **11**, 77 (2003); Ramanathan et al, Proc. 4th WCPEC (2006) p. 380]. Simulations carried out by Ana Kanevce (Fig. 1) showed decreases in the solar-cell parameters at small thicknesses. Her baseline case is based on Ramanathan's 1-μm result and is shown with circles. The minority-carrier lifetime in the absorber was taken to be 1 ns and the hole density 2 x 10^{16} cm^{-3}. At thicknesses less than 1 μm, all three solar-cell parameters decrease, and the rate of decreases becomes steeper for thickness below 500 nm.

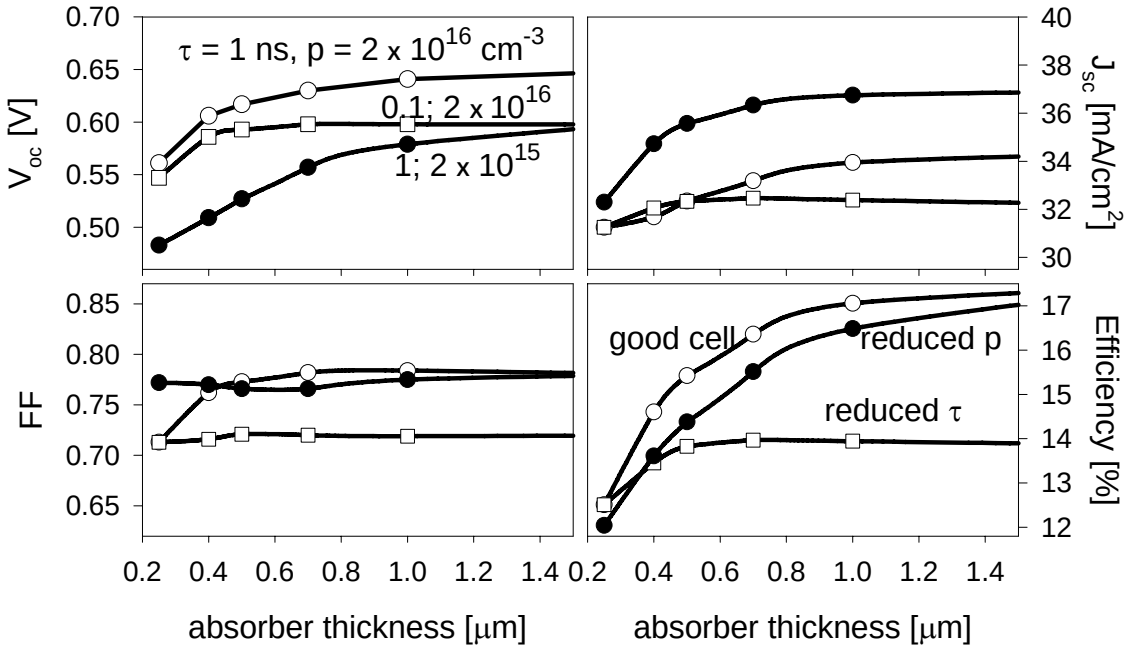

Figure 1. Calculated impact of absorber thickness on high-efficiency cell parameters (circles). Corresponding results with reduced lifetime (squares) and reduced carrier density (dots) also shown.

The calculated performance with an order of magnitude lower lifetime (squares in Fig. 1) has lower 1-μm efficiency, but a less pronounced thickness dependence except at the extremely low thicknesses (< 400 nm). Variations in minority-carrier lifetime affect

thicker devices more strongly due to their larger recombination volume. A smaller hole-density (dots in Fig. 1) also decreases the voltage, but it increases the current by about the same fraction. Below 500 nm, the calculated efficiency is be nearly independent of lifetime and hole density.

Earlier, Gloeckler and Sites [J. Appl. Phys. **98**, 103703 (2005)] showed that a key strategy for CIGS cells with absorber thicknesses below 1 μm is to limit back-contact recombination, which can be accomplished by the choice of back-contact material, surface modifications, or inclusion of grading in the Ga to In ratio. Our Phase II annual report showed (repeated as Fig. 2) that the inclusion of a simple electron reflector should substantially increase V_{oc} for thin devices. The electron reflector reduces the dominant minority-electron recombination at the back contact by keeping electrons away from it.

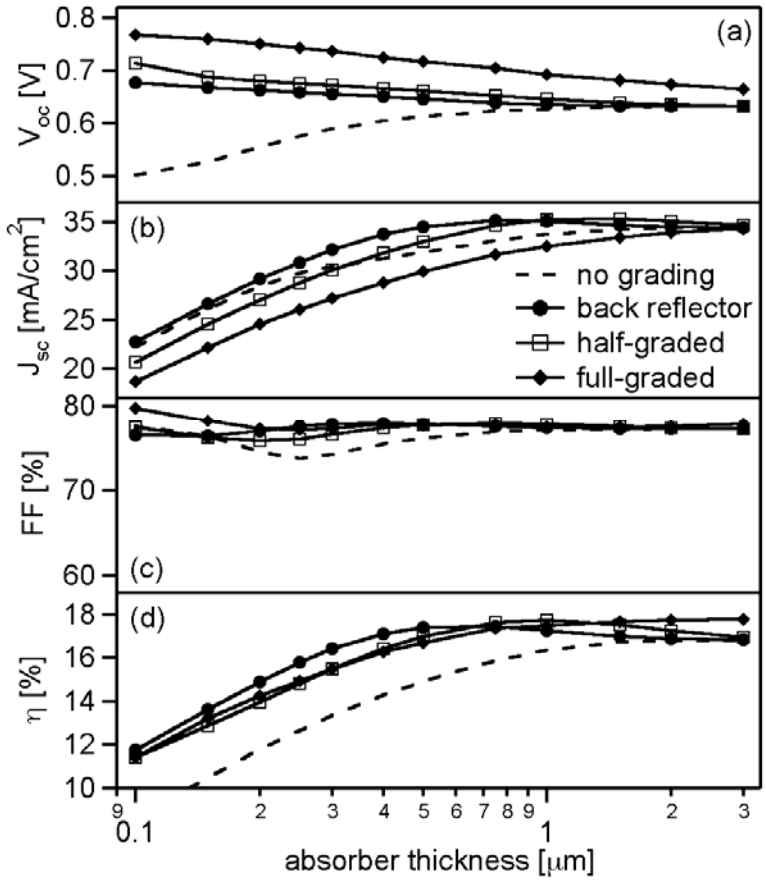

Figure 2. Performance parameters for the three grading profiles in comparison with an ungraded absorber (dashed line). ΔE_{Ba} = 0.2 eV.

The dashed lines in Fig. 2 are similar to the baseline circles in Fig. 1. As seen in Fig. 2, efficiency is essentially the same whether the reflector is formed by a band-gap expansion (more Ga) just at the back contact, or whether band-gap grading is spread over half or all of the absorber. (There is, however, a tradeoff between current and voltage when the average band gap is increased.) The recombination rate should be reduced by the same factor as the suppression of electron concentration, $\exp(-\Delta E_{Ba}/kT)$. A back grading with a band-gap increase greater than 0.2 eV reduces recombination by a factor greater than 10^3. In this situation, V_{oc} is again limited by bulk recombination, and a larger barrier height does not further increase efficiency. As the absorber is thinned, the bulk volume and hence the bulk recombination decreases, and V_{oc} may actually improve beyond that achieved in thick devices.

Another aspect of thin CIGS layers is the possibility of back-side illumination. For back-side illumination, the absorber thickness needs to be less than 1 μm for reasonable efficiency. Nakada et al [Proc. 20th EPSEC, 2005, p. 1736] have shown experimentally that reasonable efficiencies can in fact be achieved when a transparent back conductor is combined with a thin absorber.

The major difference between illumination from the front and the back side is the distribution of photogenerated carriers within the cell. With front illumination, generation occurs primarily within the space-charge region (SCR), but when a cell is illuminated from the back, most carriers are generated in the bulk part of the absorber, and most of those close to the back contact. Hence, back-contact recombination can be a very significant loss. It can, however, be significantly decreased through the choice of back-contact material and/or by increasing the Ga/In ratio, and hence the band gap, at the back of the device to produce the electron reflector.

Figure 3 shows Ana Kanevce's comparative simulations of standard solar-cell parameters for front and back illumination (circles and dots). The simulation parameters were taken from those of a high-efficiency thick cell with a 0.2-eV back-contact electron barrier.

Also shown in the efficiency plot are the data reported by Nakada et al for front and back illumination. The dashed-line fits to that data required that the absorber lifetime is reduced by a factor of ten from that of high-efficiency thick cells.

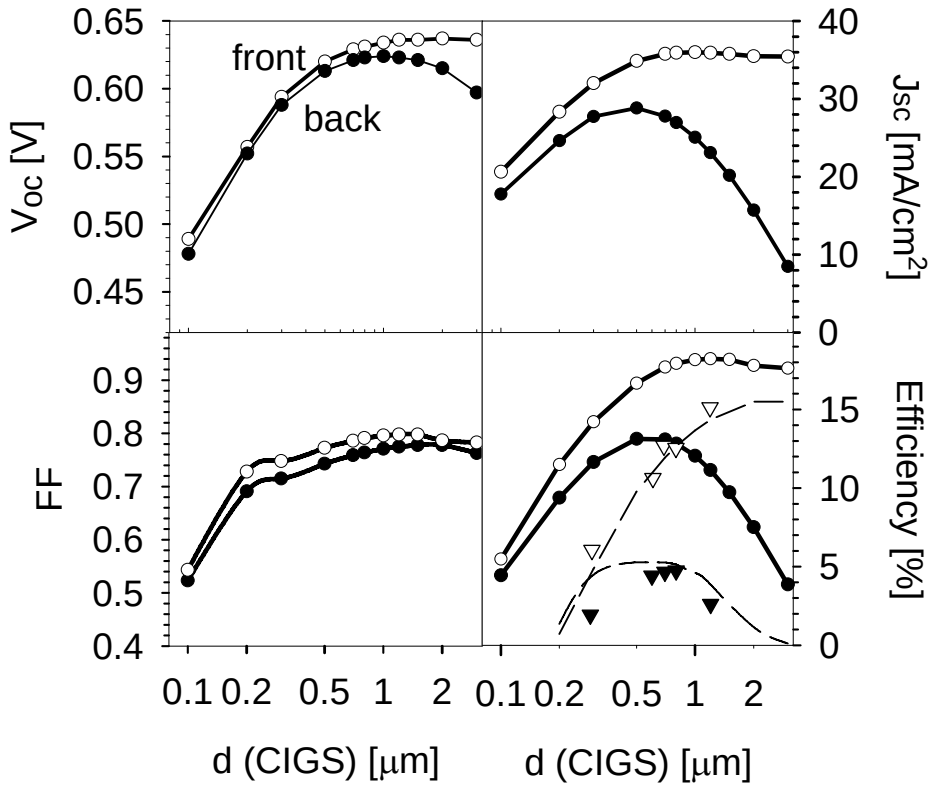

Figure 3. Calculated V_{oc}, J_{sc}, FF, and efficiency vs. absorber thickness for front (circles) and back-side (dots) illumination. Back electron reflector is assumed. Experimental data for front (open triangles) and back (filled triangles) illumination is fit by dashed lines.

Three general features to note in Fig. 3 are (1) the shape of the experimental data, particularly the back-illumination efficiency peak near 0.7 μm is similar to that seen in the calculations, (2) in the very thin-film limit (below 0.2 μm), the front- and back-illumination curves converge to the same values, and (3) the primary front/back-illumination difference for cells above 0.5 μm is seen in the current.

The current differences result from the differences in quantum-efficiency profiles, and several calculated QE curves are shown in Fig. 4. For front illumination the thinner cells lose QE at longer wavelengths as expected, and they lose a greater amount if there is no

back reflector. For back illumination of thicker cells, the QE is stronger at the longer wavelengths, but it progressively increases at the shorter ones as the absorber is thinned. The much larger difference between cells with and without a back electron reflector under back illumination is quite apparent in Fig. 4.

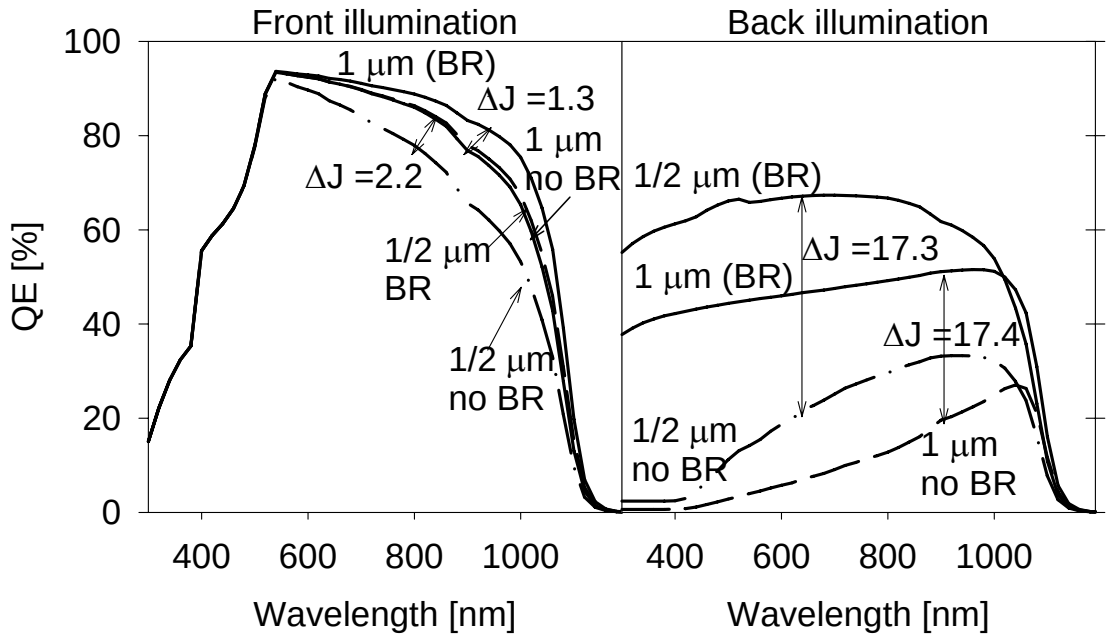

Figure 4. Quantum efficiency curves for a 1-μm and a ½-μm thick CIGS cell when illuminated from the front and from the back.

CIGS Nonuniformities. Nonuniformities in thin-film cells have been observed with several experimental techniques, and a good review of this work was presented by Karpov, Compaan, and Shvydka [Phys. Rev. B **69**, 045325 (2004)]. These studies have shown that spatial fluctuations in thin-film cells are unavoidable and generally detrimental to cell efficiency. Submicron-device performance is sensitive to variations in both material and structural parameters. In particular, thickness fluctuations impact thinner devices to an increasing degree, as can be deduced from Figs. 1 and 2. In the extreme case with fluctuations comparable to the absorber thickness, one should anticipate serious device shunting.

Nonuniformities of various types can also produce variations in the local photovoltage. For a nonuniform device, the equivalent circuit for a single diode can be replaced with a

network of diodes that may be individually defined. Numerical simulations, again performed by Ana Kanevce, used a 10 x 10 diode network, part of which is shown in Fig. 5. The baseline "strong diode" is the 1-µm, 17% cell used in Figs. 1 and 2. The back-contact resistance was assumed to be negligible compared to the transparent-conductive oxide (TCO) front-contact resistance. The resistance R between the individual diodes in the array should be proportional to the series resistance R_s of the whole solar cell. For the array illustrated here, an individual resistance of R = 3 Ω corresponds to series resistance of R_s = 1 Ω-cm^2 for the whole cell.

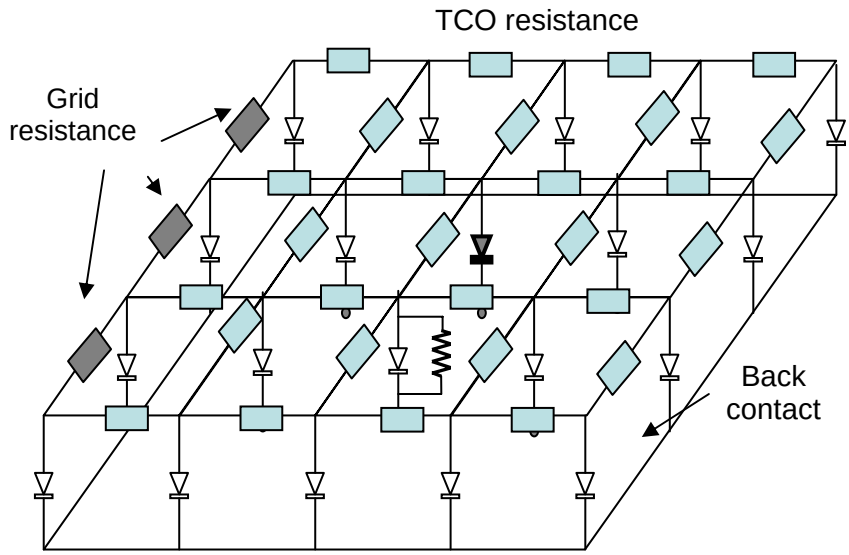

Figure 5. Schematic of diode network model. Single weak diode and shunt are highlighted.

If series resistance is neglected, a nonuniform device is a network of parallel-connected diodes with no voltage drop between adjacent diodes. The total current generated by the device is the sum of the currents through individual diodes:

$$I = \sum_{i=1}^{n} \left[I_{oi} \left(\exp\left(\frac{qV}{AkT} \right) - 1 \right) - I_{Li} \right] \qquad (1)$$

The diode quality factor A was assumed to have the same value for all the diodes, and the light-generated current I_L was assumed to be uniform throughout the device. V_{oc} for the entire device is a function of the difference between the strong V_{ocs} and the weak-diode

V_{ocw} voltage, $\Delta V_{oc} = V_{ocs} - V_{ocw}$, and of the ratio a of the weak-diode area A_w to the total device area A_t:

$$V_{oc} = V_{ocs} - \frac{AkT}{q} \ln\left[1 - a + a \cdot \exp\left(\frac{q\Delta V_{oc}}{AkT}\right)\right] \qquad (2)$$

When series resistance is finite, J-V curves cannot be calculated analytically without more substantial approximation, but the impact of the series resistance can still be calculated numerically. In the small R_s limit, numerical methods give the same results as those obtained analytically.

If TCO resistance is significant, however, it introduces a voltage drop across the TCO and thus isolates the lower-voltage area. Voltage maps $\Delta V(x,y) = V_s(x,y) - V_w(x,y)$ are shown in Fig. 6 for a small and a large value of R_s. $V_s(x,y)$ is the voltage of a uniform diode as function of position, and $V_w(x,y)$ is the voltage when 4% of the centrally located diodes have V_{oc} reduced by 0.4 V from its baseline value of 0.64 V. Although the sheet resistance in the TCO can isolate the weaker voltage areas and prevent them from dominating the entire device, it also reduces the fill-factor by a larger amount, and hence the cell's efficiency is always smaller for larger R_s.

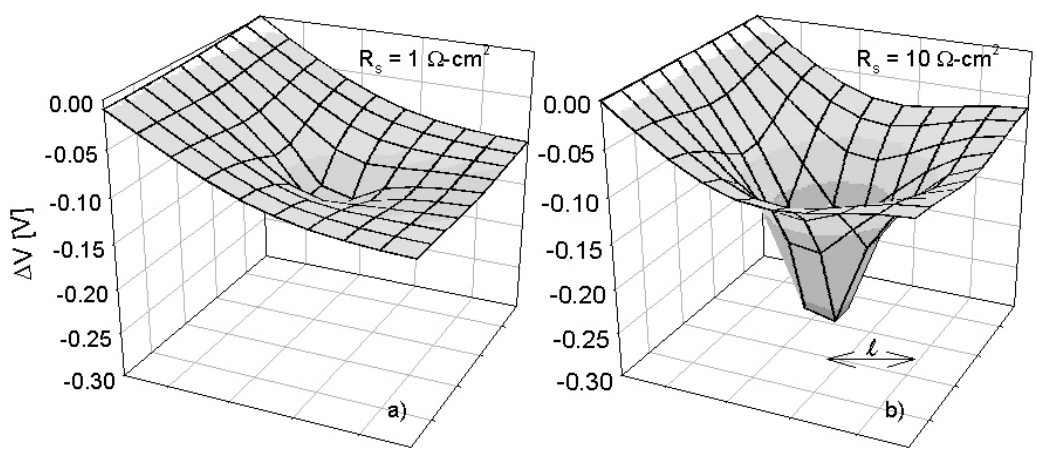

Figure 6. Voltage maps of two solar cells with different R_s. Length shown is often referred to as screening length.

The impact of a weak diode on device performance is linear in voltage and logarithmic in the area ratio to a first approximation. The calculated constant efficiency curves for a high-quality CIGS cell (17% baseline again) are shown in Fig. 7. Areas less than 10% of the total device area with voltage deficits less than 100 mV decrease the device efficiency less than 1%. A decrease of 100 mV in V_{oc} of the cell can result equally well from 0.1-eV band-gap fluctuations for any device thickness, 50% thickness fluctuation for a 250-nm thick device, or two orders of magnitude decrease in lifetime in the weak area.

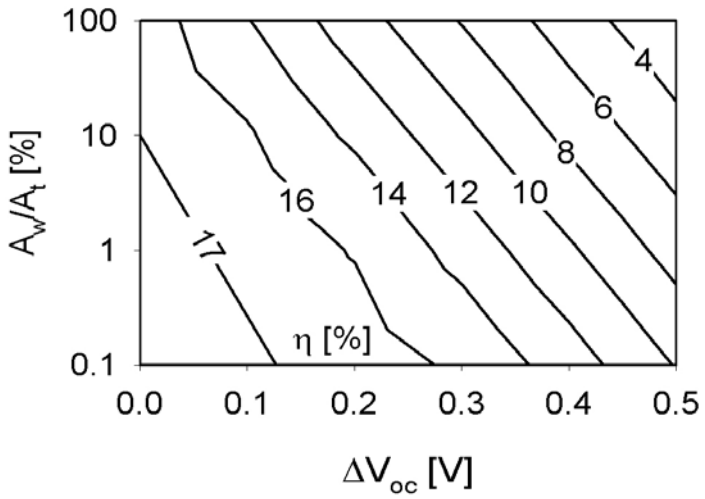

Figure 7. Efficiency dependence on ΔV_{oc} and weak area (baseline efficiency = 17%).

Since the weak diodes pull down the voltage of the nearest neighbors, the distribution of the weak diodes, as well as their area and ΔV, may affect the device voltage. Calculated results for a device with a total 4% weak-diode area showed the smallest device-voltage effect when the diodes were clustered together towards a corner of the device and the largest when they were scattered throughout the device. The maximum-power point, and thus the device conversion efficiency, however, is very nearly independent on the weak diodes' distribution.

High-Effiency CdZnS/CIGS. Ana also worked with Raghu Bhattacharya of NREL on the analysis of CIGS cells that that were fabricated with a solution-grown CdZnS buffer layer. The best of these cells achieved 19.5% efficiency, equal to that achieved with NREL's standard CdS buffer. At short wavelengths, the CdZnS buffer did achieve about

2 mA/cm^2 higher current than the CdS buffer, but it had slightly less collection in the longer wavelength region. The CdZnS buffer also produced a slightly higher A-factor (1.5 vs. 1.3) both light and dark, and is C-V curve was slightly less well behaved and indicated a smaller CIGS carrier density near the junction. A more complete report can be found in Bhattacharya et al, Appl. Phys. Lett. **89**, 253503, (2006).

BASIC CdTe STUDIES

Voltage Deficit. The highest reported efficiency for thin-film CIGS solar cells is 3% larger than the highest seen with CdTe cells. Band-gap considerations alone would predict a 3% difference in the opposite direction. The lower CdTe efficiency is primarily the result of a much larger voltage deficit between CdTe cells and crystalline cells of similar band gap.

Figure 8 compares J-V curves from record-effiency CIGS and CdTe cells with those of high-efficiency single-crystal Si and GaAs. The latter were adjusted slightly (30-40 mV in voltage, about 1 mA/cm^2 in current density) for consistency with the CIGS and CdTe band gaps.

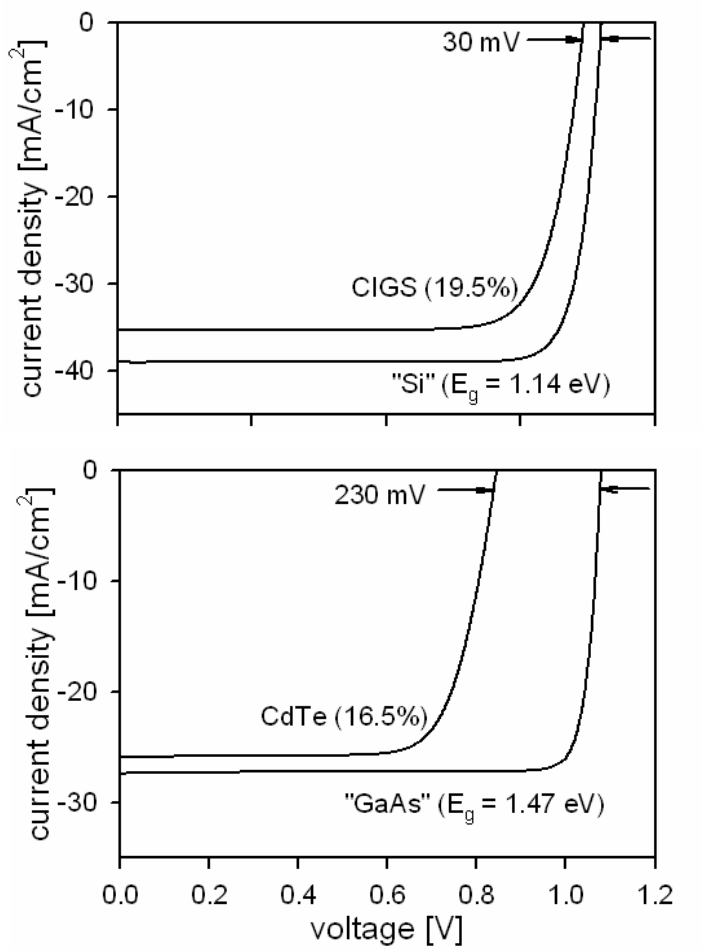

Figure 8. J-V Comparison of record CIGS cell with high-efficiency Si, adjusted slightly for band gap (top). Similar comparison of CdTe with GaAs (bottom).

The salient feature of Fig. 8 is the 230-mV voltage deficit for CdTe compared to the 30 mV deficit for CIGS. The CIGS voltage deficit is in fact remarkably small. One explanation is that Cu-deficiency near grain boundaries (GBs) results in a lowered valence band [Persson and Zunger, Phys. Rev. Lett. , 2003] which repels holes from the GBs [Gloeckler et al, JAP, 2005]. No comparable effect likely with CdTe. Reduction of the CdTe deficit to that of CIGS would increase CeTe cell efficiency by about 5% to approximately 22%. The obvious questions are why does such a large difference exist between the CdTe and the CIGS voltage deficit and what might be done to significantly reduce the CdTe deficit.

Two distinctly different approaches for increasing CdTe voltage, which will be referred to as the "n-p" and the "n-i-p" strategies, were examined. Figure 9a shows the band diagram of a CdTe solar cell with a thin n-CdS window layer. The low CdTe hole density ($2x10^{14}$) in Fig. 9a is typical of today's cells and makes the CdTe absorber intermediate between i-type (intrinsic) and p-type. As a consequence, the depletion region extends over a large fraction, but not all, of the CdTe thickness. The possibility of a significant back-contact barrier Φ_b is indicated by the dashed line. That possibility was evaluated in some detail during Phase I, but here the valence band will be assumed to be flat (the solid line in Fig. 9a).

Figure 9b, where the hole density is increased to $2x10^{17}$, is the classic n-p hetero-junction. It is similar to what one would find with n-on-p GaAs, and we will explore what needs to be altered about the polycrystalline CdTe to achieve performance comparable to GaAs. In contrast, Fig. 9c lowers the hole density to $2x10^{13}$, the CdTe becomes fully depleted, and terminology used here is n(CdS)-i(CdTe)-p(back of CdTe). This configuration can also lead to high voltage, but of major importance in this case is the presence of an electron reflector Φ_e at the rear on the absorber. As with the n-p configuration, the question for the n-i-p approach is what specifically needs to be done to achieve high voltage and efficiency.

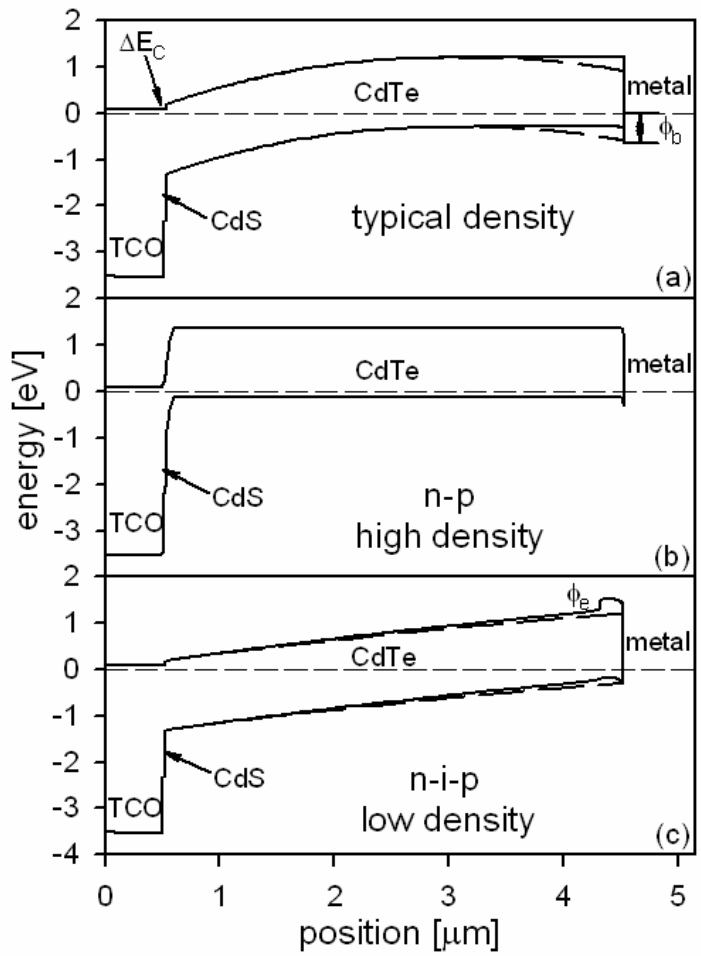

Figure 9. (a) Typical CdTe cell with and without a significant back-contact barrier. (b) Significantly higher hole density. (c) Lower density with and without an electron reflector.

CdTe voltage was calculated by Jun Pan as a function of the CdTe recombination lifetime τ for the three situations shown in Fig. 9. Figure 10 shows graphically that both high lifetime and high carrier density would be required for a high voltage in the n-p configuration. Physically, a reduction in the density of defects could be the key to improvements in both: increased lifetime through a smaller number of recombination centers and increased carrier density through a smaller number of compensating states. One risk, however, is that CdS/CdTe is a heterojunction with the potential for interfacial recombination, which could become the voltage-limiting factor if the bulk CdTe properties were significantly improved.

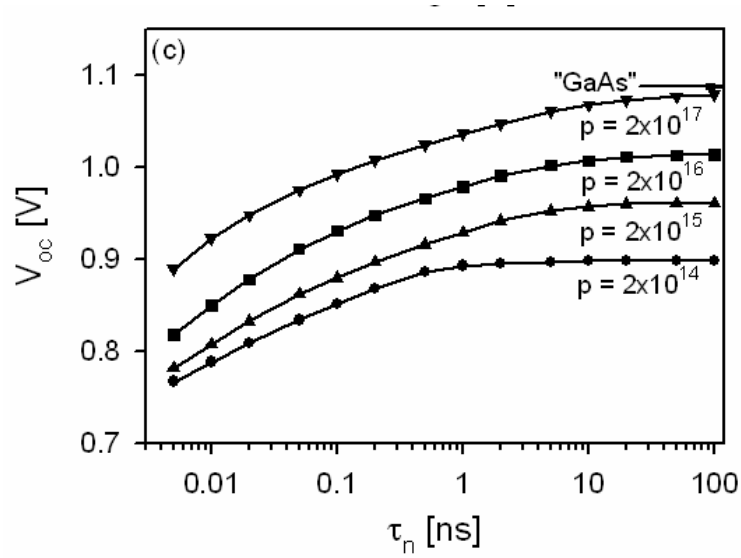

Figure 10. CdTe n-p cell needs major increases in both carrier density and lifetime.

Calculated voltages for the p = $2x10^{13}$ fully-depleted absorber configuration (Fig. 9c) are shown in Fig 11. In this case, a conduction-band barrier near the back surface, often referred to as an electron reflector, is critical to reduce voltage-limiting recombination at the back surface. Without this increase, denoted Φ_e, the voltage is slightly lower than that of the typical $2x10^{14}$ carrier-density CdTe, but with even a small back reflector (0.2 eV), the voltage should increase significantly. Higher values of Φ_e lead to only modest additional improvement, and the thickness and carrier density of the reflector layer lead to only minor variations in the J-V curves.

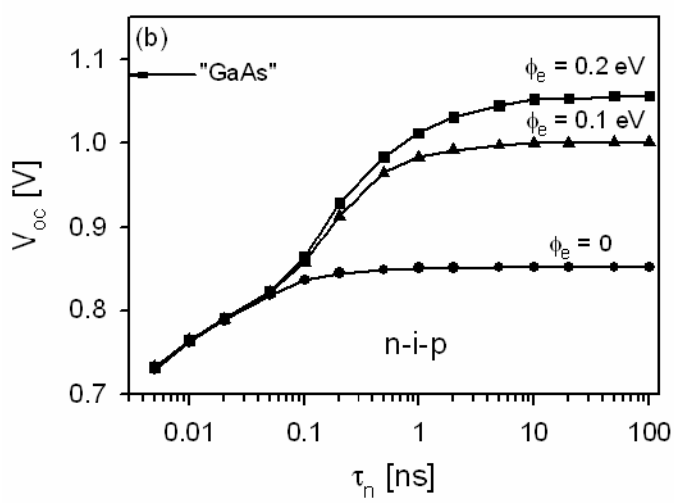

Figure 11. CdTe n-i-p requires a back electron reflector and modest lifetime.

Figure 11 shows that when the electron-reflector barrier is present, the lifetime need not be particularly high. One possibility for creating such a barrier is to add a layer of ZnTe or other material with an expanded gap in the conduction-band direction. A potential difficulty, however, is that any recombination at the CdTe/ZnTe or other reflector interface will compromise the advantage of keeping electrons away from the metal interface. If an electron barrier is applied to CdTe that is not fully depleted, the benefit is relatively small, because the carrier densities at the back would not be large enough for back recombination to significantly lower the voltage.

Figure 12 summarizes the two approaches to increasing CdTe voltage. The simulated n-p J-V curve corresponds to substantial increases in CdTe lifetime and hole density. As shown, the n-p curve has a voltage of 1080 mV and an efficiency of 22% even if current losses in today's record cell are not reduced. The n-i-p simulation yields a somewhat similar J-V curve with a voltage of 1030 mV and an efficiency of 21% at a moderate lifetime of 2 ns. It does require an electron reflector the order of 0.2 eV in height near the back contact. It may well be the more promising strategy for improving voltage and performance, since it should not require a major improvement in the quality of thin-film CdTe to reach one volt and 20%.

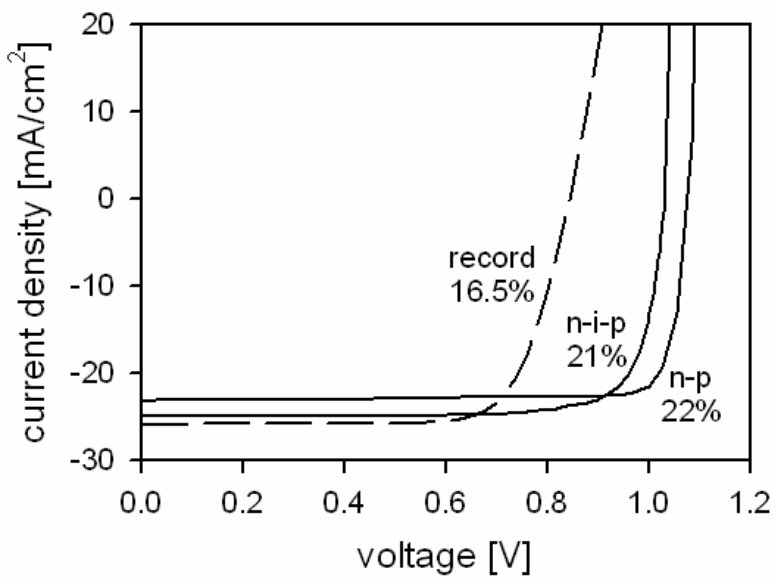

Figure 12. Comparison of record-cell J-V curve with possible major improvements using n-p and n-i-p strategies

Absorber Lifetime. The minority carrier lifetime of CdTe, which was the key parameter for the voltage calculations shown in Figs. 10 and 11, also has a strong influence on the solar-cell fill-factor (Fig. 13). From Jun Pan's calculations, the short-lifetime collection of photogenerated carriers, even those generated within the depletion region's electric field, is increasingly incomplete in forward voltage where the field is reduced. At higher lifetimes, essentially all carriers generated in the depletion region will be collected, and hence the dependence of collection on voltage becomes very small.

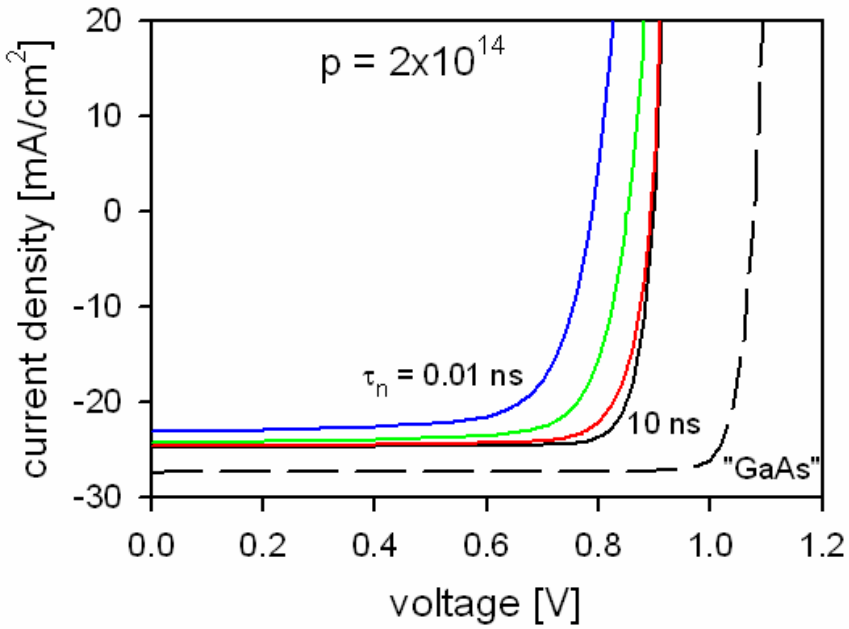

Figure 13. Calculated J-V for typical-carrier-density CdTe as a function of minority carrier lifetime, again referenced to GaAs prediction.

One analytical consequence of the low-lifetime curves in Fig. 13 is that they are no longer exponential, and the calculation of a well defined diode quality A fails. If one ignores the non-exponential behavior and attempts to calculate A, the voltage-dependent collection inherently overestimates its value. The result is shown in Fig. 14 where A = 1, light and dark, for large lifetimes where the forward diode current results from thermionic emission. At smaller lifetimes, bulk recombination becomes significantly larger, and the A-factor should transition to a Shockley-Reed-Hall value of 2, or slightly less if the distribution of recombination states varies though the absorber. This is the case in the dark, where the J-V curve is unaffected by changes in photocarrier collection with voltage. In the light, however, the voltage-dependent-collection effect on the J-V curves

yields artificial A-values well above 2 for the very short lifetimes an artificially enhanced A-values for typical CdTe-cell lifetimes.

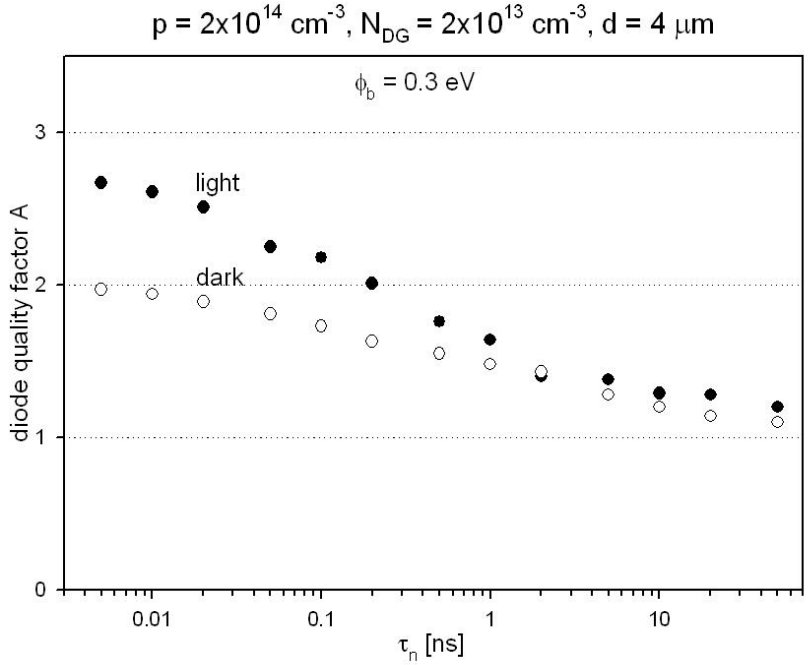

Figure 14. Artificial enhancement of A-factor at small lifetimes.

Experimental curves from cells with different CdTe lifetimes are shown in Fig. 15. The measurements were made by Samuel Demtsu working in collaboration with David Albin at NREL. In this case, lifetime variations result from different amounts of copper used in the formation of the back contact. There is more than one effect seen in the Fig. 15 curves. With no copper at all, the back-contact barrier is significant, and thus the curve rolls over in the first quadrant and the fill-factor is reduced. With a small amount of copper, the back barrier is reduced, and the J-V curve is quite good. With additional copper, however the absorber lifetime is reduced, and the fill-factor is again smaller.

Experimental lifetime can be deduced from time-resolved photoluminescence (TRPL) measurements. TRPL from the same cells depicted in Fig. 15 were made by Wyatt Metzger at NREL and are shown in Fig. 16. Room-temperature capacitance-voltage measurements, also made on the same cells, showed an increase in net carrier density and a decrease in depletion width with increased amounts of Cu. Hence, we conclude that the

use of copper helps the cell by reducing the back barrier, but it also introduces additional acceptors accompanied by a decrease in hole lifetime. A minimal amount of copper appears to be optimal for efficiency.

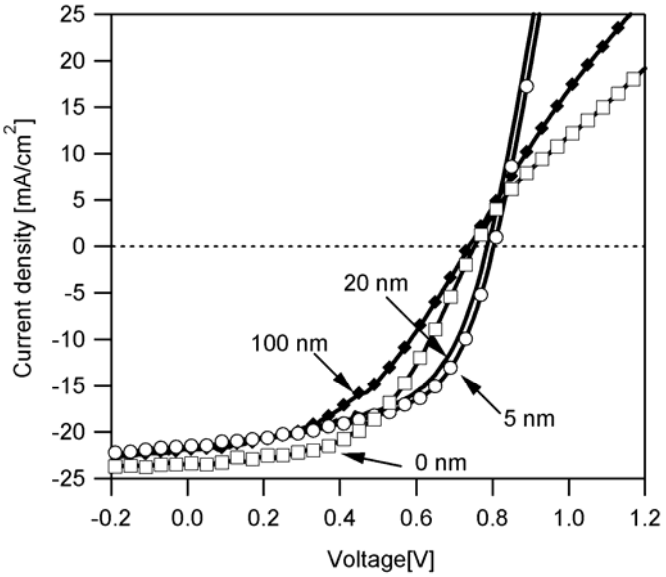

Figure 15. CdTe J-V curves for cells with different amounts of back-contact copper.

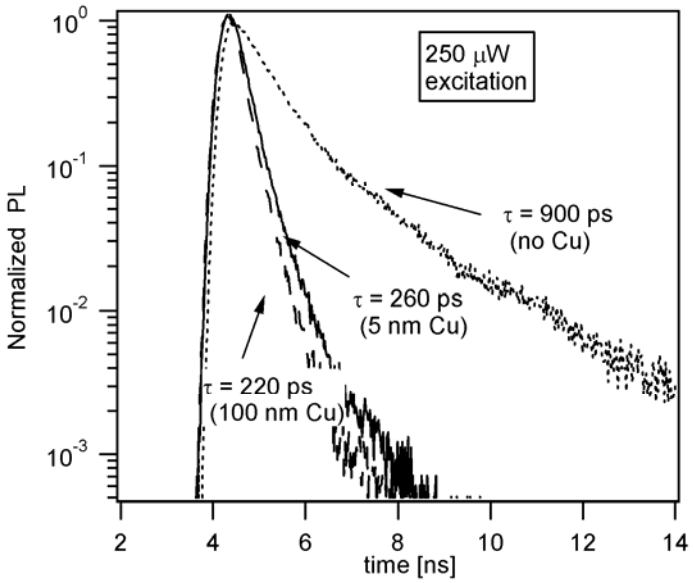

Fig. 16. Normalized CdTe TRPL decay curves as a function of Cu thickness.

Thin CdS. Several thin-film CdS/CdTe solar cells were fabricated with Prof. Sampath's in-line CSS pilot deposition line at Colorado State University. Quantum efficiency

measurements were performed by Alan Davies to ascertain CdS layer thicknesses, identify the degree of CdS/CdTe intermixing (small), and estimate the absorber band-gap (about 1.47 eV for all of the cells). QE curves for eight devices (Fig. 17) show the variation in CdS thickness among thedevices sampled. From the QE data in the 400-500 nm range, we estimated optical CdS thicknesses ranging from about 10 to 240 nm. Also evident from QE curves is a modest decrease in collection of photogenerated carriers in the thinner CdS cells for wavelengths near the band-gap. This decrease can reasonably be attributed to a shorter electron lifetime for thin-CdS devices

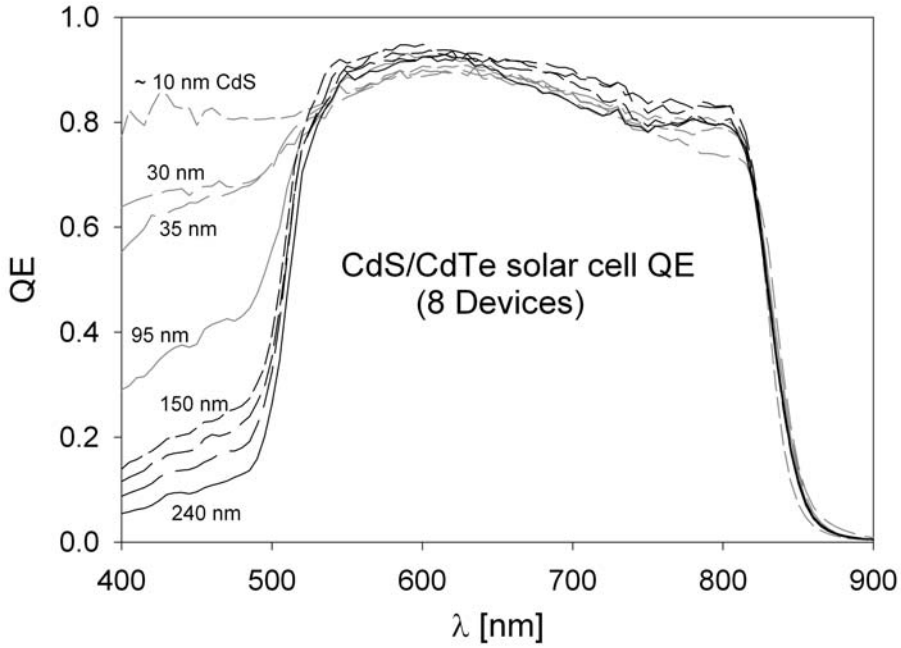

Figure 17: Variation of CdS/CdTe QE response with CdS thickness.

Figure 18 shows all three J-V parameters for the same cells used for the Fig. 17 QE curves. Efficiencies, which are between 10 and 12% for devices with thicker CdS, fall into the 3 to 6% range once the CdS thickness is significantly below 100 nm. Immediately evident is the increase in J_{sc} with thinner CdS resulting from the increased transmission as CdS is thinned. Also obvious is the sharp drop in V_{oc} and increase in J_o between 100 and 50 nm. As CdS thickness decreases, CdS pin-hole formation is likely to become more prevalent, and consequently J_o and V_{oc} would approach values that may correspond to a SnO_2/CdTe photodiode.

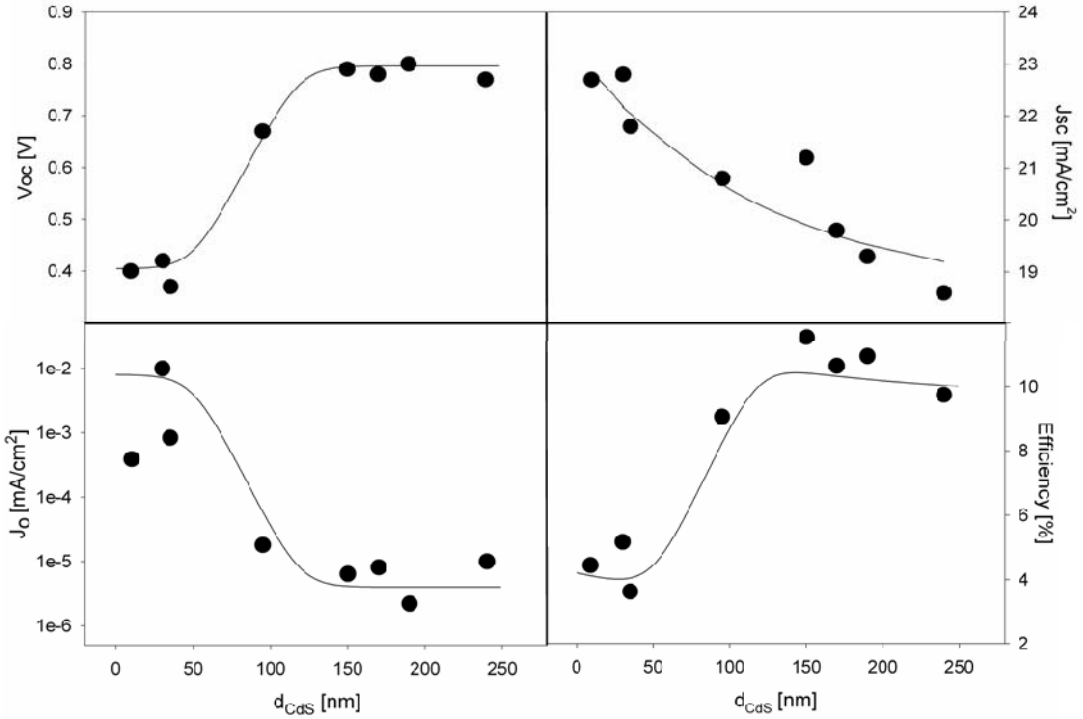

Figure 18: J-V parameters, plotted against CdS layer thickness, show overall performance loss below 100 nm.

The concept of pinholes exposing the CdTe directly to the SnO_2 window layer strongly suggests that the thin-CdS cells should have a significantly less uniform photovoltaic response. This predicted contrast in uniformity is clearly seen in the Fig. 19 LBIC scans, which show a broadening of local QE by about twenty times.

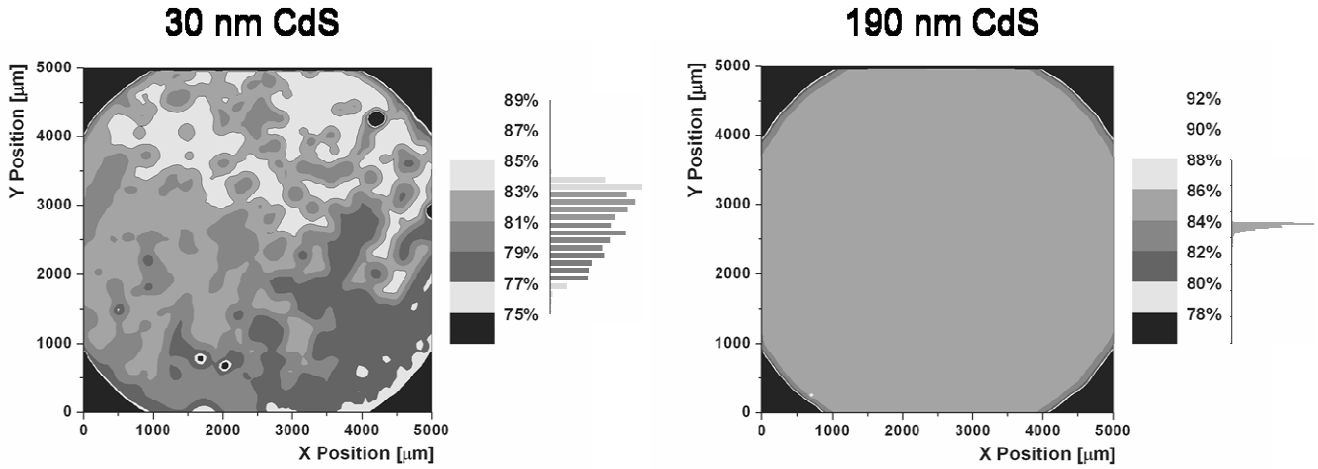

Figure 19. LBIC comparison of thin and intermediate-thickness CdS.

GENERAL STUDIES

QE Under Light Bias. During Phase II, we have very carefully recalibrated our quantum-efficiency system, refined the software and procedures for efficient data collection, and installed the capability a white-light bias of variable intensity. Much of the QE improvement was done by an undergraduate student, Jacob van der Vliet, who compared several reference-cell candidates and made cross-calibrations with reference cells measured at NREL. He also made several improvements to the QE measurement protocol and several upgrades to the software used to store and display the QE results.

At the same time, Tim Nagle and Alan Davies have investigated different light sources and controls to apply white bias light during QE measurement. As with other researchers, they found that the QE curve can be affected by the presence of bias light. In many cases as shown in Fig. 19, the change is small, it only effects QE near the CdTe band gap, and it saturates with a modest amount of bias light. Nevertheless, it is a real effect that is quite reproducible. Its likely explanation is that a secondary effect of CdS photoconductivity is a small increase in the CdTe depletion width under illumination, which improves the collection of electrons generated deep in the CdTe.

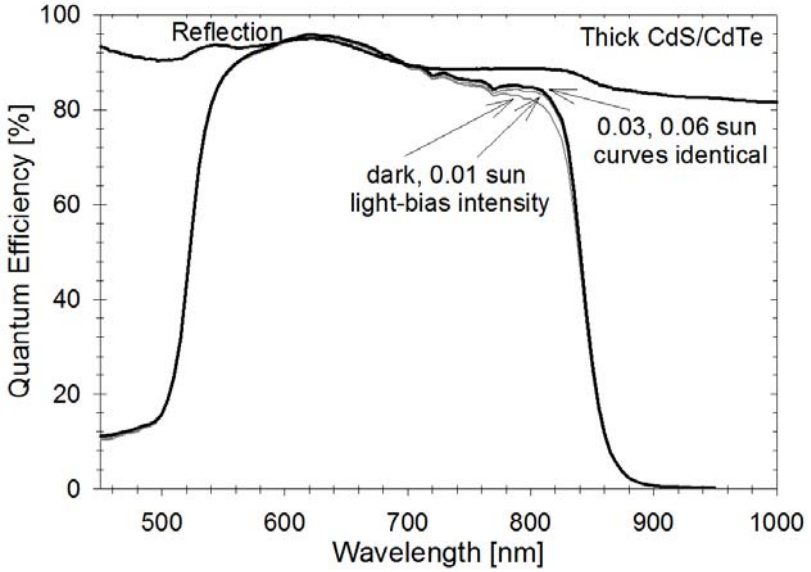

Figure 19. Small bias-light effect on measured CdS/CdTe QE.

In some cases, however, the effect of bias light can be much more dramatic. For example, a poor-efficiency CIGS yielded the QE curves shown in Fig. 20. The light-bias effect is very large and is not saturated at 5% of standard solar intensity. The J-V curve (inset) suggests a large conduction-band offset ("spike") at the CdS/CIGS interface. Such a barrier would block photogenerated electrons unless there are sufficient blue photons absorbed in the CdS to lower the interfacial barrier.

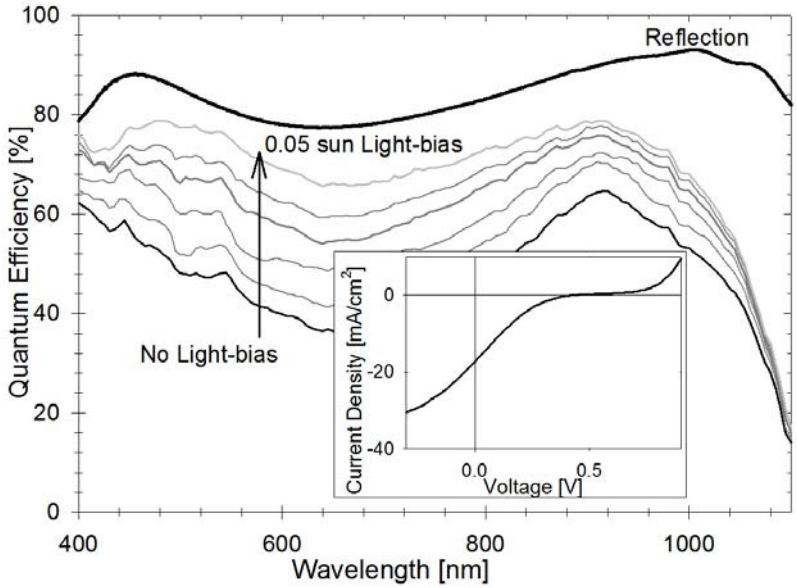

Figure 20. Strong QE dependence on bias-light suggests a large secondary barrier in the CdS/CIGS conduction band, an observation supported by the J-V curve.

We would like to be able to apply a stronger bias light and have found that six-volt krypton "Mag-lite" bulbs are a suitable white-light source with an intensity that can be varied up to half a sun. Furthermore, they are small enough to be mounted in our QE system without extensive modification. The next step, which will be implemented by Simon Kocur, a visiting student from Regensburg, Germany, is to design and build a mount so that the bulb-to-cell distance can be varied over a sufficientrange that the bias intensity can be reproducibly varied in steps from 1% to 50% of solar intensity.

Effective Module Efficiency. A joint project with Marko Topič and his colleagues at the University of Ljubljana in Slovenia has calculated the effective efficiency of PV modules averaged over a year under various field conditions. This is an important issue, because

field conditions are almost never the same as the standard test conditions (STC) commonly used to rate modules. Depending on the specific module parameters and the field conditions, the actual power over the course of a year can vary significantly from that predicted by the STC rating.

In the absence of variations in temperature or illumination spectrum, and when the series resistance and the leakage conductance in a PV module are negligible, the module efficiency η increases roughly logarithmically with solar irradiation. The primary factor is the open-circuit voltage V_{OC} and its direct effect on the fill-factor. The V_{OC} vs. irradiation curve, however must be adjusted for the module's temperature coefficient, its effective series resistance, and its effective leakage conductance.

The increase in CIGS module temperature with irradiance P, compared to the ambient temperature, is very nearly linear and to has essentially the same proportionality constant for many commercial modules. This temperature coefficient dT_c/dP is also very similar for many of the commercially-available modules of different technologies, and it is approximately 30ºC/kW-m^{-2}. The temperature effect reduces $\eta(P)$ by an amount also very nearly proportional to irradiance. The effective series resistance R_s per cell and the effective leakage conductance G_{sh} do vary considerably among modules, but can generally be deduced from a manufacturer's data sheets. R_s has a larger effect at higher irradiance, while G_{sh} per cell reduces the module efficiency in inverse proportion to irradiance. The overall result is that the maximum efficiency for many modules occurs in the neighborhood of one-half sun. The details will vary with the technology employed and with the values of dT_c/dP, and effective R_s and G_{sh} for the specific module under consideration. Simulation of the a-Si and CdTe modules is slightly more complicated than for CIGS, because the effective G_{sh} may change significantly with irradiance.

The annual effective efficiency η_{eff} can be defined as a ratio of integrated available electrical energy generated in a year divided by the integrated solar energy. The process formally requires site-specific temperature and irradiance data, but the result does not

depend strongly on the site selected. In general, η_{eff} is smaller η_{STC}, the often-specified efficiency corresponding to one sun and 25°C, and the ratio can vary as much as 10% among modules. As a practical matter, we found that measurement of module efficiency at one half-sun intensity gives a reasonably reliable value for the annual average for a wide variety of commercial PV modules.

Industrial Impact. The primary industrial impact has been that PhD graduates have become professional staff members at various PV companies. During Phases I and II, Alex Pudov joined Nanosolar, Markus Gloecker went to First Solar, Samual Demtsu was hired by SoloPower, and Caroline Corwine is now part of Advent Solar. In addition, several of the current students have formed relationships with PV companies, and former student Ingrid Eisgruber Reppins has returned to the active PV community to work at NREL.

More directly, Tim Nagle and the other students have been working with industrial partners in three primary ways: (1) measurement and analysis of specific cells in our lab (Heliovolt, and Nanosolar), (2) advice for building or refining in-house systems for J-V and QE measurements (ISET and Heliovolt), and (3) supplying analysis and simulation software and consulting on its use (Solyndra, Heliovolt, and Miasole). In several cases, we have agreed to not publicly discuss details of the measurements or the results of these activities.

PHASE III PLANS

Much of the work planned for Phase III will follow smoothly from that reported above. The Phase III work will involve continued collaboration with our team partners, and it will continue to focus on both specific and basic-science information needed to assist with the commercialization of thin-film photovoltaics. During Phase III, we should achieve completion for several of the ongoing projects:

(1) Thin CIGS absorbers, including the comparison of the expected J-V and QE curves with experimental results, the analysis of non-uniformity effects, and the response to back-side illumination.

(2) Strategies for increasing the voltage and collection efficiency of CdTe cells, including specific proposals for experimental implementation of the n-p and n-i-p approaches.

(3) The effects of thinner CdS with CdTe cells, including the need for a TCO bilayer and the relation to copper migrating from the back contact.

(4) Full implementation of variable-intensity white-light bias as a photovoltaic measurement and analysis tool; continued development of the Colorado State LBIC facility.

We will also continue our assistance to thin-film PV companies with the measurement and analysis of individual CIGS and CdTe cells of interest. During Phase III, four students (Ana Kanevce, Jun Pan, Tim Nagle, and Alan Davies) should complete their PhD degrees. Second-year student Galym Koishiyev and first-year student Lei Chen will continue. In addition, Simon Kocur, visiting from Germany, and senior collaborators Alan Fahrenbruch and Marko Topič will assist with the various projects.

COMMUNICATIONS

Publications

(1) J. Pan, M. Gloeckler, and J.R. Sites, "Hole-Current Impedance and Electron-Current Enhancement by Back-Contact Barriers in CdTe Cells," J. Appl. Phys. **100**, 124505, (2006).

(2) S.H. Demtsu and J.R. Sites, "Effect of Back-Contact Barrier on Thin-Film CdTe Solar Cells," Thin Solid Films **510**, 320-324 (2006).

(3) S.H. Demtsu, D.S. Albin, J.W. Pankow, and A.R. Davies, "Stability Study of CdS/CdTe Solar Cells Made with Ag and Ni Back Contacts," Solar Energy Materials and Solar Cells **90**, 2934-2943 (2006).

(4) M. Topič, K. Breel and J.R. Sites. "Performance Assessment of PV Modules – Relationship Between STC Rating and Field Performance," Proc. World Conf. on Photovoltaic Energy Conversion **4**, 2141-2144 (2006).

(5) A.L. Fahrenbruch, "The Relationship of CdS/CdTe Band Profiles to J-V Characteristics," Proc. World Conf. on Photovoltaic Energy Conversion **4**, 376-379 (2006).

(6) S. Demtsu, D.Albin, and J.R. Sites, "Role of Copper in the Performance of CdS/CdTe Solar Cells," Proc. World Conf. on Photovoltaic Energy Conversion **4**, 523-526 (2006).

(7) M. Topič, K. Brecl, J. Kurnik, and J. Sites, "Effective Efficiency and Performance Ratio as Energy Rating System for PV Modules," Proc. E-PVSEC **21**, 2507-2510 (2006).

(8) D.S. Albin, S.H. Demtsu, and T.J. McMahon, "Film Thickness and Chemical Processing Effects on the Stability of CdTe Solar Cells," Thin Solid Films **515**, 2659-2668 (2006).

(9) R. N. Bhattacharya, M.A. Contreras, B. Egaas, R. Noufi, and A. Kanevce, and J.R. Sites. "High Efficiency Thin Film $CuIn_{1-x}Ga_xSe_2$ Photovoltaic Cells Using a $Cd_{1-x}Zn_xS$ Buffer Layer," Appl. Phys. Lett. **89**, 253503, (2006).

(10) M. Topič, K. Breel, and J.R. Sites, "Effective Efficiency of Photovoltaic Modules Under Field Conditions," Progress in Photovoltaics, **15**, 19-26 (2007).

(11) S.H. Demtsu, D.S. Albin, J.R. Sites, W.K. Metzger, and A. Duda. "Cu-Related Recombination in CdTe Solar Cells," Thin Solid Films, in press.

(12) J.R. Sites and J. Pan, "Strategies to Increase CdTe Solar-Cell Voltage," Thin Solid Films **515**, 6909-6102 (2007).

Presentations

(1) Jim Sites, "Device Physics and Numerical Simulation: Routes to Understanding CdTe and CIGS Cells," University of Delaware, February 21, 2006.

(2) Jim Sites, "Basic Solar-Cell Measurements," Heliovolt Corporation, Austin, TX, March 1, 2006.

(3) Jim Sites, Jun Pan, and Markus Gloeckler, "Impact of Lifetime and Back-Contact Barrier on CdTe Current-Voltage Curves: Simulation of Commonly Seen Features," CdTe Team Meeting, Golden, March 9, 2006.

(4) Alan Davies, "Effect of Cu and $CdCl_2$ on Stability," CdTe Team Meeting, Golden, March 9, 2006.

(5) Caroline Corwine, "Compensating Cu/O Complex in CdTe," CdTe Team Meeting, Golden, March 9, 2006.

(6) Alan Fahrenbruch, "Photoconductive CdS and Anomalous QE Effects: Comparison of Experiment and Modeling," CdTe Team Meeting, Golden, March 9, 2006.

(7) Jim Sites, "Can V_{OC} in CdTe Cells Be Increased Significantly?" CdTe Team Meeting, Golden, March 10, 2006.

(8) Markus Gloeckler, "Potential for Thin-Film CIGS: a Device Study," CIS Team Meeting, Golden, April 6, 2006.

(9) Ana Kanevce, "Predicted Behavior of Cells with Thin CIGS Absorbers," CIS Team Meeting, Golden, April 6, 2006.

(10) Alan Fahrenbruch, "The Relationship of CdS/CdTe Band Profiles to J-V Characteristics," WCPEC-4, Kona, Hawaii, May 12, 2006.

(11) Jim Sites and Jun Pan, "Strategies to Increase CdTe Solar-Cell Voltage," E-MRS, Nice, France, May 31, 2006.

(12) Jim Sites, "Why are There Large Differences in CdTe J-V Curves?" SOLARPACT Meeting, Nice, France, June 2, 2006.

(13) Jim Sites, "CIGS: Four Grain-Boundary Possibilities," Grain-Boundary Workshop, Frejus, France, June 3, 2006.

(14) Jim Sites, "Device Physics and Numerical Simulation: Routes to Understanding CIGS and CdTe," University of Ljubljana, Slovenia, July 6, 2006.

Graduate Degrees

(1) Caroline Corwine (PhD, August 2006), Thesis, "Role of Cu-O Defect in CdTe Solar Cells."

(2) Samuel Demtsu (PhD, August 2006), Thesis: "Impact of Back-Contact Materials on the Performance and Stability of CdS/CdTe Solar Cells."

(3) Galym Koishiyev (MS, January 2007), coursework degree.